Available online at www.sciencedirect.com
ScienceDirect
Journal of Power Sources 180 (2008) 294–300
JOURNAL OF POWER SOURCES
www.elsevier.com/locate/jpowsour

Low-temperature sintering of lanthanum strontium manganite-based contact pastes for SOFCs

B.P. McCarthy [a], L.R. Pederson [a,*], Y.S. Chou [a], X.-D. Zhou [a], W.A. Surdoval [b], L.C. Wilson [c]

[a] *Pacific Northwest National Laboratory, P.O. Box 999, Richland, WA 99352, United States*
[b] *National Energy Technology Laboratory, 626 Cochrans Mill Road, Pittsburgh, PA 15236-0940, United States*
[c] *National Energy Technology Laboratory, 3610 Collins Ferry Road, Morgantown, WV 26507-0880, United States*

Received 5 January 2008; received in revised form 25 January 2008; accepted 25 January 2008
Available online 23 February 2008

Abstract

Electrical contact pastes of composition $(La_{0.90}Sr_{0.10})_{0.98}MnO_{3+\delta}$ (LSM-10) formed strong bonds (~3 MPa) to $(Co,Mn)_3O_4$ spinel-coated Crofer 22 APU ferritic steel coupons when exposed to alternating flows of air and nitrogen (10 ppm O_2) at 900 °C for 2 h or longer. When held at 900 °C in air only, bond strengths were negligible. Substantial bonds could also be created between LSM-10 contact paste and $(La_{0.80}Sr_{0.20})_{0.98}MnO_{3+\delta}$ (LSM-20) porous cathodes by processing in alternating air and nitrogen, without simultaneous densification of the cathode. Enhanced sintering of LSM-10 is attributed to transients in the defect structure induced by oxygen partial pressure changes.

Keywords: Lanthanum strontium manganite; Contact paste; Oxygen partial pressure cycling; Enhanced shrinkage; Sintering; Solid oxide fuel cell

1. Introduction

Non-negligible losses due to contact resistance between metallic interconnect plates and ceramic electrodes have been observed in planar solid oxide fuel cells (SOFCs), the result of resistive interfacial scale formation as well as low contact area [1–4]. Contact resistance losses on the anode side are small, where nickel metal pastes and nickel mesh are typically utilized to provide a low-resistance metallurgical bond between the nickel-based anode and a metallic interconnect. It is more challenging to achieve low-resistance contacts on the cathode side, where at least one ceramic-metal interface and possibly several ceramic–ceramic interfaces are present.

To inhibit the growth of a resistive scale and to decrease chromium volatilization, a variety of protective coatings have been applied onto metallic interconnects. Perovskite coatings have been most widely studied, including unsubstituted and Sr-substituted $LaCoO_3$ [5–11], $LaFeO_3$ [8], $LaMnO_3$ (LSM) [1,8,10,12,13], and $LaCrO_3$ [9,10,12,13]. Low-resistance contacts were also obtained with $LaNi_{0.6}Fe_{0.4}O_3$ coatings [14], which offer the advantage of relatively low-processing temperatures. Spinel coatings, particularly $(Mn,Co)_3O_4$, have provided favorable electrical properties and good long-term stability [1,8,9,15].

Because mechanical (unbonded) contacts between even quite conductive materials can be both highly resistive and non-linear [16], augmentation of the coated interconnect/cathode interface may be necessary in an SOFC. The application of a mechanical load can lower the resistance of unbonded ceramic contacts, which for LSM follows relatively steep power law dependence [17]. The variability in mechanical load in an SOFC stack with thermal cycles and over time presents challenges in using this approach to manage contact resistance. Good electrical contact can also be facilitated by the introduction of a contact paste between the cathode and coated interconnect. That contact material should either be compliant or provide a good thermal expansion match to other fuel cell components, exhibit high-electrical conductivity, provide good interfacial stability, and be of low cost, among other attributes. It is also preferred that the contact paste be processed at temperatures compatible with

* Corresponding author. Tel.: +1 509 375 2731.
E-mail address: larry.pederson@pnl.gov (L.R. Pederson).

0378-7753/$ – see front matter © 2008 Elsevier B.V. All rights reserved.
doi:10.1016/j.jpowsour.2008.01.097

that at which glass seals are typically formed (850–1050 °C [18–21]).

Either noble metals or conductive ceramics could serve as the contact paste. Noble metals such as platinum, silver, and gold present a cost disadvantage. Platinum and silver also have been observed to electromigrate, which may alter cathode performance [22]. LSM generally meets contact paste material requirements, with the exception of a higher than desired air sintering temperature. A processing temperature of 1200 °C was required for an air-side electrical connector produced by infiltration of a carbon fiber cloth with an LSM slurry, for example [13]. It is possible to lower the sintering temperature of LSM through partial substitution of cobalt for manganese and through tailoring of the particle size distribution [23]. McCarthy et al. [24] recently demonstrated that sintering of $(La_{0.90}Sr_{0.10})_{0.98}MnO_{3+\delta}$ (LSM-10) occurred substantially faster when exposed to alternating exposure to air and to nitrogen (10 ppm O_2) than in air for temperatures <∼1000 °C. Enhanced sintering was attributed to the transient co-existence of cation and oxygen vacancies, which increased mobility. In this paper, principles given by McCarthy et al. [24] have been applied to the processing of LSM-based contact pastes at low temperature.

2. Experimental methods

Combustion synthesis was used to produce the powders for this study, where an aqueous solution containing metal nitrates and glycine was concentrated and then combusted to yield a fine ash composed of the desired oxides [25]. An A-site deficiency of 2% was used to avoid the formation of a separate lanthanum oxide phase. The ash was calcined at 1250 °C to volatilize any remaining organics and to convert the powder to a single crystalline phase. A particle size of ∼1 μm was achieved by ball milling for 8–12 h with zirconia milling media in isopropanol. Once the desired particle size was achieved, as measured using a Horiba LA-920 laser particle size analyzer, the powder/isopropanol mix was dried and gathered. The gathered powder was subjected to X-ray diffraction (Philips 3100 XRG) to verify the phase purity of the powder. Representative sintered samples were additionally dissolved in dilute hydrochloric acid and analyzed by inductively coupled argon plasma spectroscopy (Agilent 4500 Series) to verify the overall composition of LSM samples.

Dilatometry studies of pre-sintered LSM-10 and LSM-20 bars were conducted to compare the sintering behavior of these compositions in alternating air (0.21 atm O_2, 1 h) and nitrogen (∼10^{-5} atm O_2, 1 h) in the temperature range 700–1200 °C. Shrinkage rates were also measured in air in the temperature range 1000–1400 °C. Below 1000 °C, shrinkage rates in air were at or below detection limits. Bars were made by uniaxially pressing LSM powders to 12 MPa. Up to 70% weight carbon was added as a pore former. The bars were heated to 1250 °C at 3 °C min^{-1}, and then held at that temperature for 2 h. Once pre-sintered to the desired density, the bars were sectioned into smaller samples ∼2.2 cm × 0.3 cm × 0.3 cm in dimension for dilatometry studies (Anter Unitherm Model 1161). Densities were determined via the Archimedes method.

The alloy used in this study was Crofer 22 APU, a ferritic stainless steel that was developed by Forschungszentrum Jülich and produced by ThyssenKrupp VDM GmbH specifically for SOFC interconnect applications [26]. Coupons approximately 1 cm × 1 cm were coated with a protective $(MnCo)_3O_4$ spinel layer via spray coating to control scale growth, following procedures described by Yang et al. [8].

To simulate possible procedures used in SOFC production, screen-printing and pneumatic dispensing application methods were employed to apply LSM-10/polyvinyl butyral (PVB, 17:3 weight ratio) inks to Crofer 22 APU coupons. To achieve an acceptable final contact material thickness, ink was applied to one side of two spinel-coated Crofer 22 APU coupons using an automated screen printer (DEK Model 248) and allowed to dry at 100 °C for 30 min. The dried ink was nominally 20 μm in thickness. Ink of a similar thickness was reapplied to one coupon and pressed, wet, against the second dried ink-covered coupon. LSM-10/PVB inks were also applied via a syringe using an EFD 1500XL pneumatic dispenser in a single-step, with the wet ink pressed between the first and second coupons.

Thermal processing of steel/contact paste/steel sandwich specimens consisted of repeated and alternating exposure to air (0.21 atm O_2, 10 min) and to nitrogen (∼10^{-5} atm O_2, 10 min) at 900 °C within a closed-ended tube furnace at 900 °C. These conditions were shown by McCarthy et al. [24] to result in a local maximum in the rate of densification of LSM-10. During processing, the coupons were subjected to a uniaxial force of 35 kPa perpendicular to the plane of the contact paste. Thermal processing times of up to 10 h were employed. A second set of coupons was exposed to air only for similar processing times. Densification rates of pre-sintered LSM-10 and LSM-20 bars (initially ∼55% of theoretical density) was also assessed by dilatometry (Anter Unitherm 1161 equipped with Ono Sokki EG-225 LVDT displacement gauges that provide a resolution of ±0.001 mm) in both alternating air–nitrogen and in air as a function of temperature.

The fracture strength of Crofer 22 APU coupons (∼1 cm × 1 cm) bonded with LSM-10 contact paste was evaluated in tension (MTS Materials Testing Systems Bionix 400). The metal coupons were attached with epoxy to a self-aligning grip fixture. Measurements were performed at room temperature using a cross-head speed of 0.5 mm min^{-1}. Four to seven samples were tested for each condition.

3. Results and discussion

3.1. Densification of pre-sintered LSM-10 and LSM-20

Preliminary to bonding strength studies, rates of densification of pre-sintered LSM-10 and LSM-20 bars were evaluated as a function of temperature when alternately exposed to air and nitrogen (10^{-5} atm O_2). For LSM-10 pre-sintered to 55% of theoretical density, repeated cycling between air (1 h) and nitrogen (1 h) resulted in enhanced rates of densification for temperatures less than ∼1000 °C when compared to an extrapolation of rates obtained in air only, as shown in Fig. 1. Shrinkage rates were determined from a minimum of five air–nitrogen cycles, dur-

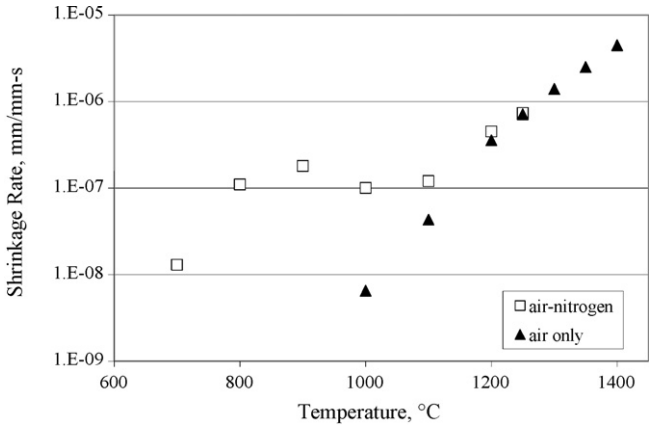

Fig. 1. Shrinkage rates measured using dilatometry for LSM-10 bars initially 55% dense that were exposed to either alternating air (1 h) and nitrogen (1 h) or to flowing air at the indicated temperatures. Densification rates at low temperature in alternating air and nitrogen were enhanced, the result of changing oxygen non-stoichiometry and cation vacancy concentrations.

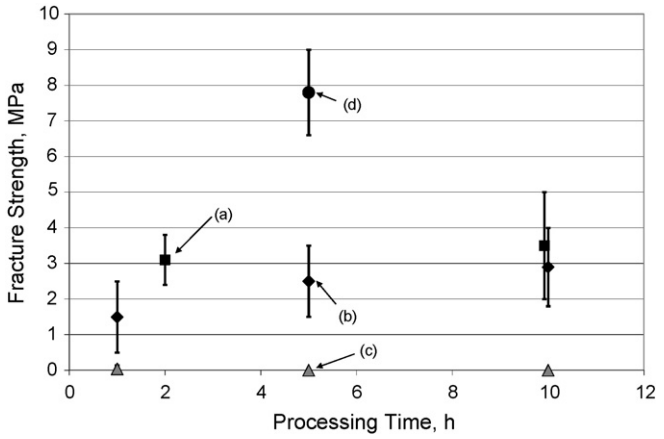

Fig. 3. (a) Tensile fracture strength for two spinel-coated Crofer 22 APU coupons bonded together with 50 μm thick LSM-10 contact paste at 900 °C in alternating air (5 min) and nitrogen (5 min); (b) same as (a) except 10 μm thick LSM contact paste; (c) same as (a) except processed in flowing air; (d) tensile strength of LSM-10 to single steel coupon.

ing which the extent of shrinkage per cycle remained constant. Shrinkage rates in air at temperatures less than 1000 °C were too low to be measured reliably, consistent with previous observations [27,28]. For temperatures of ∼1100 °C and above, rates measured in alternating air–nitrogen and in air were similar. McCarthy et al. [24] related this behavior to changes in oxygen non-stoichiometry in LSM-10, which results in the transient co-existence of cation and oxygen vacancies above equilibrium concentrations.

For LSM-20 samples pre-sintered to an initial density of 58% of theoretical, air–nitrogen cycles led to modest, if any, enhanced densification, as given in Fig. 2. The extent of oxygen non-stoichiometry in LSM-20 in air is diminished compared to that in LSM-10 [29,30], so smaller changes in oxygen and cation vacancy concentrations are expected during air–nitrogen cycles.

It thus appears possible to sinter an LSM-10 contact paste under conditions that would not simultaneously densify the

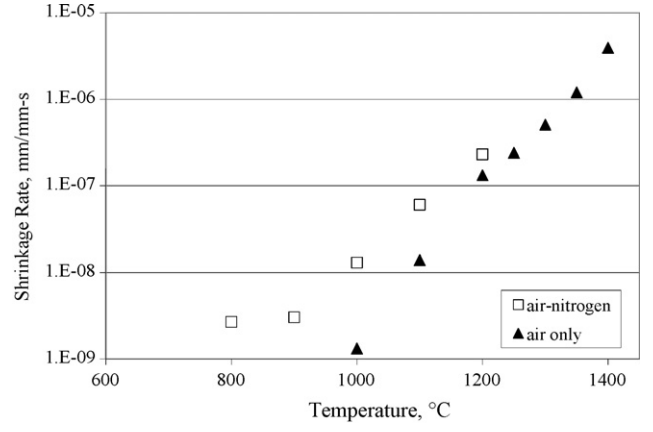

Fig. 2. Shrinkage rates measured using dilatometry for LSM-20 bars initially 58% dense that were exposed to conditions identical to those of Fig. 1. Densification rates were minimally enhanced in alternating air and nitrogen for LSM-20, which exhibits a lower extent of oxygen non-stoichiometry than LSM-10.

LSM-20 cathode. Further, LSM-10 and LSM-20 are chemically compatible and show very similar thermal expansion behavior (11.2 and 11.3 ppm K^{-1}, respectively [31]). The electrical conductivity of LSM-10 is adequate for use as a contact paste, though less than that of LSM-20 (∼80 S cm^{-1} for LSM-10 versus ∼120 S cm^{-1} for LSM-20 in air at 800 °C [32]). The key issue addressed here is whether this approach can be used to form sufficiently strong, low-resistance bonds to the cathode and to the interconnect plate within a practical time at temperatures consistent with glass seal processing.

3.2. LSM-10 bonding to spinel-coated Crofer 22 APU

Substantial bonds between spinel-coated Crofer 22 APU ferritic steels and LSM-10 contact pastes were created by repeated cycles of alternating exposure to air and nitrogen, as shown in Fig. 3 and summarized in Table 1. Thermal processing was performed at 900 °C, shown previously to give the greatest enhancement in sintering of LSM-10 in alternating oxygen and nitrogen exposure [24]. A cycle time of 20 min (10 min in flowing air followed by 10 min in flowing nitrogen) was used, also consistent with conditions that resulted in the highest sintering rates [24]. Bond strengths did not change significantly for processing times greater than 2 h. Alternating air–nitrogen cycles clearly are critical to the formation of strong bonds with LSM-10: samples processed in air at 900 °C developed negligible bond strengths. A cross-section of a typical coated interconnect-LSM-10 contact material-interconnect sandwich specimen processed for 2 h at 900 °C in alternating air an nitrogen is given in Fig. 4, which shows extensive sintering within the paste itself and a continuous bond to the spinal coating. The relative density of the contact paste in Fig. 4 was estimated by image analysis to be 65 ± 3% (ImageJ [33]), whereas the green density was 41 ± 3%. Specimens processed in air only for similar times at that temperature were quite fragile, and typically fractured while handling.

Table 1
Fracture strength results for spinel-coated Crofer 22 APU coupons bonded with LSM-10 contact paste at 900 °C

Number of samples	Sintering condition/paste thickness (μm)	Fracture strength (MPa)	Note
4	1 h, air–nitrogen/∼10	1.5 ± 1.0	Fractured within contact paste
5	2 h, air–nitrogen/∼50	3.1 ± 0.7	Fractured within contact paste
5	5 h, air–nitrogen/∼10	2.5 ± 1.0	Fractured within contact paste
4	10 h, air–nitrogen/∼50	2.9 ± 1.1	Fractured within contact paste
5	10 h, air–nitrogen/∼10	3.5 ± 1.5	Fractured within contact paste
5	1 h, air only/∼10	0.04 ± 0.1	4 of 5 samples fractured on loading
4	5 h, air only/∼10	0.0 ± 0.0	All samples fractured on loading
4	10 h, air only/∼10	0.0 ± 0.0	All samples fractured on loading
7	5 h, air–nitrogen/∼10	7.8 ± 1.2	LSM-10 to Crofer 22 APU bond strength, failed at epoxy/Al fixture interface

Fracture in specimens processed in alternating air and nitrogen occurred inter-granularly within the porous LSM-10 contact material, rather than at the contact paste/coated interconnect interface. Thus, bond strengths given in Fig. 3 really reflect the mechanical properties of the porous contact material and not the interfacial bond. Incomplete paste coverage for some of the samples also effectively lowered measured bond strengths and increased experimental scatter. Apparent bond strengths are substantially smaller than have been reported for fully dense LSM compositions. For LSM-12.5, at a room temperature three-point bend strength of 164 MPa was reported, for which failure occurred trans-granularly [34]. A biaxial flexure strength of ∼50 MPa was determined for LSM-20 at ambient temperature [35], with similar results obtained for $La_{0.5}Sr_{0.5}Mn_{0.96}Co_{0.04}O_{3+\delta}$ [36]. It is well-known that the strength of porous ceramics decreases sharply with increased porosity, such as following the empirical relation [37]:

$$\sigma = \sigma_o \exp(-nP) \quad (1)$$

where σ, σ_o are fracture strengths of porous and fully dense materials, n is in the range of 4–7, and P is the porosity fraction. For a porosity volume fraction of 0.35, consistent with the contact paste microstructure of Fig. 4, the strength is estimated to be 9–25% of values determined for fully dense samples. Because strength is largely controlled by flaw size, which can vary widely with processing conditions for a given composition, strength values reported here are not directly comparable to literature results. However, the observation that fracture strengths for bonded metal coupons are smaller than estimated from Eq. (1) and literature results for fully dense materials suggest that improvements in bond strengths are possible.

In an alternate approach to evaluate the interfacial bond strength, a single, spinel-coated steel coupon was coated with LSM-10 paste and processed in alternating air–nitrogen as previously described. In this case, the aluminium test fixture on one side was bonded directly to the sintered LSM-10 paste with epoxy. The fracture strength that was obtained was nearly 8 MPa, more than double that for metal/contact paste/metal sandwich specimens, the results of which are included in Fig. 3 and Table 1. Further, fracture occurred at the LSM-10/epoxy interface, so the actual LSM-10/spinel-coated Crofer 22 APU bond strength may well be even higher.

3.3. Bonding of LSM-10 contact paste to porous LSM-20 cathode

An LSM-10 contact paste was used to bond a spinel-coated Crofer 22 APU coupon to a porous LSM-20 film, which had been screen-printed onto a dense LSM-20 disk. This test fixture approximates the configuration that may be employed in a planar SOFC stack, and is similar to that described previously by Yang et al. [8]. A cross-section of a sample that had been

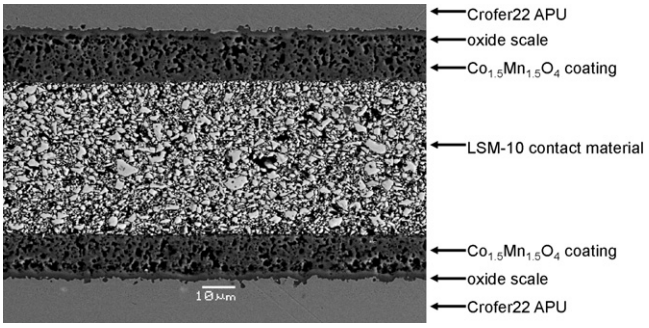

Fig. 4. Cross-section of two $Co_{1.5}Mn_{1.5}O_4$ spinel-coated Crofer 22 APU coupons bonded together with screen-printed LSM-10 contact paste and heat-treated for 2 h at 900 °C in alternating air (10 min) and nitrogen (10 min).

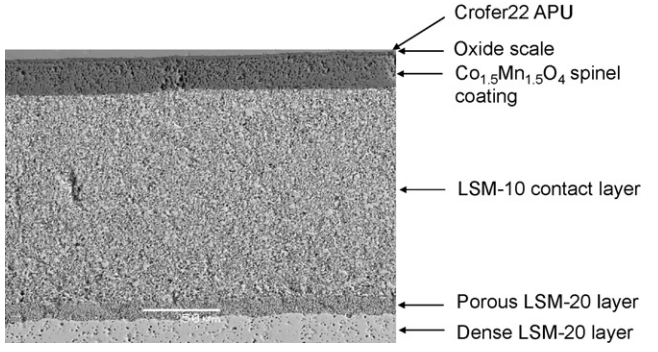

Fig. 5. Polished cross-section of a $Co_{1.5}Mn_{1.5}O_4$ spinel-coated Crofer 22 APU coupon bonded to porous LSM-20 by LSM-10 contact paste. The contact paste was thermally processed in alternating air (10 min) and nitrogen (10 min) at 900 °C for 5 h.

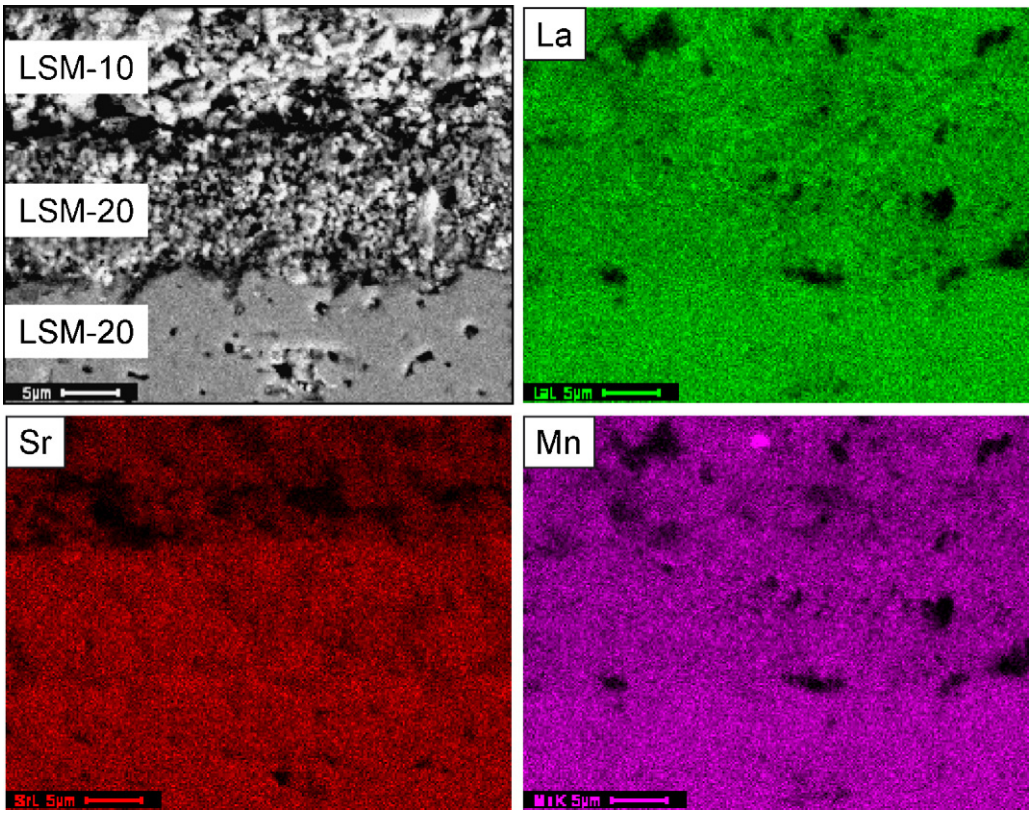

Fig. 6. Elemental maps obtained by energy dispersive spectroscopy of the dense LSM-20/porous LSM-20/LSM-10 contact material interfaces.

subjected to alternating air (10 min) and nitrogen (10 min) for 2 h at 900 °C is shown in Fig. 5. A sharp, well-bonded interface formed between the LSM-10 contact paste and porous LSM-20, with no obvious physical imperfections. The LSM-20 film retained its smaller particle size and porosity (~60% relative density), while the LSM-10 contact paste sintered to approximately 65% relative density, as estimated using image analysis. Elemental maps of the LSM-10/LSM-20 interface given in Fig. 6 show an abrupt change in the strontium concentration, while lanthanum and manganese concentrations are relatively uniform, as expected. Similarly, the LSM-10 interface with $(Co,Mn)_3O_4$ spinel revealed a well-bonded interface absent of obvious imperfections. Elemental maps of this interface, which are given in Fig. 7, show sharp compositional boundaries with no indication

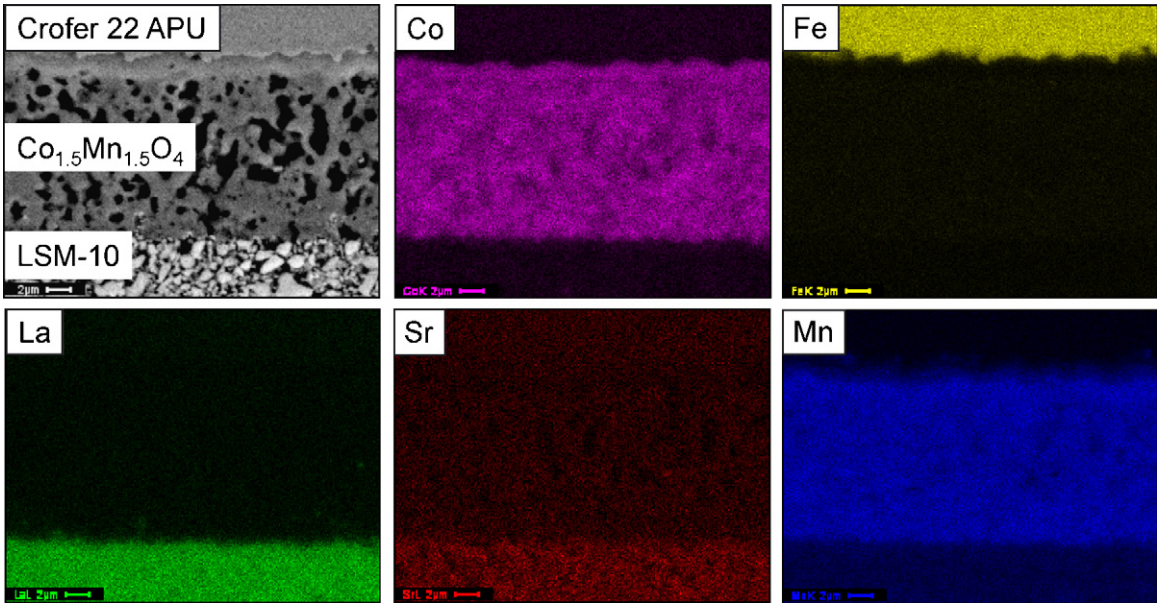

Fig. 7. Elemental maps obtained by energy dispersive spectroscopy of the Crofer 22 APU-$Co_{1.5}Mn_{1.5}O_4$ spinel coating-LSM-10 contact material interfaces.

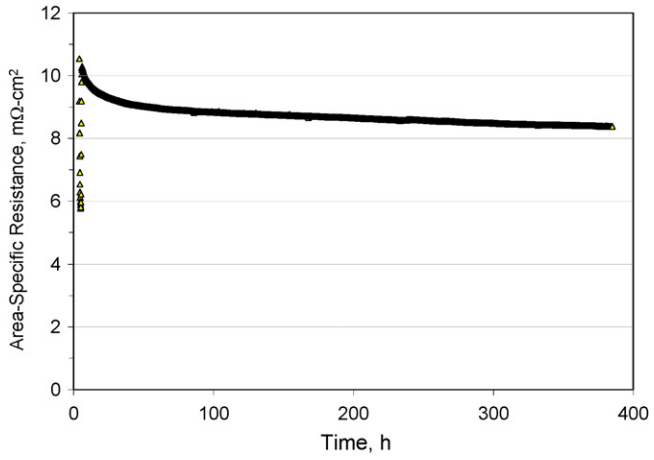

Fig. 8. Electrical resistivity of spinel-coated Crofer 22 APU/LSM-10 contact paste/spinel-coated Crofer 22 APU sandwich specimen versus time, measured in air at 800 °C.

of extensive interdiffusion or the formation of new interfacial phases.

3.4. Electrical properties

With no evidence of either new phase formation or extensive interdiffusion at interfaces, it is expected that LSM-10 contact paste would contribute minimally to the overall resistance of cells and stacks. An empirical expression was given by Hale [38] to account for the effects of porosity:

$$\rho_{\text{porous}} = \frac{\rho_{\text{bulk}}}{1-(3/2)\,P} \quad (2)$$

where ρ_{porous}, ρ_{bulk} are resistivities of porous and bulk materials, the resistivity. Assuming a bulk resistivity for LSM-10 of 0.0125 Ω cm [32], a porosity fraction of 0.35, and a contact paste thickness of 50 μm, a negligible additional resistance of 0.25 mΩ cm^2 is estimated using Eq. (2). The electrical resistivity of an interconnect/paste/interconnect sandwich specimen configured as shown in Fig. 4 was evaluated as a function of time at 800 °C, as is given in Fig. 8. The resistivity was initially ~10 mΩ cm^2, and improved throughout the test. As concluded previously, electrical properties of such specimens tend to be dominated by the development of an oxide scale on the ferritic steel [1,8,15], so contributions due to the contact paste are difficult to assess directly. The magnitude and stability of the electrical resistivity, though preliminary, suggests that this approach may offer a promising alternative to processing contact pastes for SOFCs.

4. Conclusions

Air–nitrogen cycling has been shown to be a viable means of sintering LSM-10-based contact pastes at 900 °C. Substantial interfacial bonds of at least 3 MPa to $(Co,Mn)_3O_4$ spinel-coated Crofer 22 APU ferritic steel coupons were developed within approximately 2 h at 900 °C. The bond strength of LSM-10 to the $(Co,Mn)_3O_4$ spinel coating was determined to be at least 8 MPa. When contact pastes were processed in air, bond strengths developed between steel coupons were negligible. A reasonably low (<10 mΩ cm^2) and stable resistivity over several hundred hours for spinel-coated ferritic steel and LSM-20 coupons bonded with LSM-10 contact paste that was processed at 900 °C in alternating air–nitrogen.

LSM-20 cathodes are not appreciably densified under conditions where LSM-10 contact pastes can be processed effectively. This behavior is related to differences in the extent of oxygen non-stoichiometry, as has been described by McCarthy et al. [24]. Oxygen deficient cathode compositions such as substituted lanthanum cobaltites, lanthanum ferrites, or lanthanum cobalt iron oxides similarly would not be expected to exhibit enhanced sintering in alternating air and nitrogen. As such, it may be possible to form strong bonds to ferrite and cobaltite-based cathode materials by selectively densifying LSM-10 contact pastes at relatively low temperatures.

Acknowledgements

The authors gratefully acknowledge support from the US Department of Energy, Office of Fossil Energy's Solid State Energy Conversion Alliance (SECA) Coal-Based Systems Core Technology Program. The authors appreciate helpful discussions with SP Simner, JW Stevenson, P Singh, and ZG Yang, and are indebted to GG Xia for performing an assessment of electrical properties of contact pastes. Research was supported by the US Department of Energy, Office of Fossil Energy, Solid State Energy Conversion Alliance (SECA) Coal-Based Systems program. Pacific Northwest National Laboratory (PNNL) is operated by Battelle for the US Department of Energy under Contract AC06 76RLO 1830.

References

[1] W.J. Quadakkers, J. Piron-Abellan, V. Shemet, L. Singheiser, Mater. High Temp. 20 (2003) 115–127.
[2] W. Schafer, A. Koch, U. HeroldSchmidt, D. Stolten, Solid State Ionics 86–88 (1996) 1235–1239.
[3] W.Z. Zhu, S.C. Deevi, Mater. Res. Bull. 38 (2003) 957–972.
[4] L.G.J. de Haart, K. Mayer, U. Stimming, I.C. Vinke, J. Power Sources 71 (1998) 302–305.
[5] T. Shiomitsu, T. Kadowaki, T. Ogawa, T. Maruyama, in: M. Dokiya, O. Yamamoto, H. Tagawa, S.C. singhal (Eds.), Fourth International Symposium on Solid Oxide Fuel Cells (SOFC-IV), vol. PV 95-1, Electrochemistry Society, Pennington, NJ, 1995, pp. 850–857.
[6] H.P. Buchkremer, U. Diekmann, L.G.J. de Haart, H. Kabs, U. Stimming, D. Stover, in: U. Stimming, S.C. Singhal, H. Tagawa, W. Lehnert (Eds.), Fifth International Symposium on Solid Oxide Fuel Cells (SOFC-V), vol. PV 97-40, Electrochemical Society, Pennington, NJ, 1997, pp. 160–170.
[7] W.J. Quadakkers, H. Greiner, M. Hansel, A. Pattanaik, A.S. Khanna, W. Mallener, Solid State Ionics 91 (1996) 55–67.
[8] Z.G. Yang, G.G. Xia, P. Singh, J.W. Stevenson, J. Power Sources 155 (2006) 246–252.
[9] Y. Larring, T. Norby, J. Electrochem. Soc. 147 (2000) 3251–3256.
[10] Y. Yoo, M. Dauga, in: H. Yokokawa, S.C. Singhal (Eds.), Seventh International Symposium on SOFC (SOFC-VII), vol. PV 2001-16, Electrochemical Society, Pennington, NJ, 2001, pp. 837–846.
[11] O. Teller, W.A. Muelenberg, F. Tietz, E. Wessel, W.J. Quaddakkers, in: H. Yokokawa, S.C. Singhal (Eds.), Seventh International Symposium on

SOFC (SOFC-VII), vol. PV 2001-16, Electrochemical Society, Pennington, NJ, 2001, pp. 895–903.
[12] R. Ruckdaschel, R. Henne, G. Schiller, H. Greiner, in: U. Stimming, S.C. Singhal, H. Tagawa, W. Lehnert (Eds.), Fifth International Conference on Solid Oxide Fuel Cells (SOFC-V), vol. PV 97-18, Electrochemical Society, Pennington, NJ, 1997, pp. 1273–1282.
[13] K. Murata, M. Shimotsu, J. Ceram. Soc. Jpn. 111 (2003) 222–226.
[14] R.N. Basu, F. Tietz, O. Teller, E. Wessel, H.P. Buchkremer, D. Stover, J. Solid State Electrochem. 7 (2003) 416–420.
[15] P.E. Gannon, C.T. Tripp, A.K. Knospe, C.V. Ramana, M. Deibert, R.J. Smith, V. Gorokhovsky, V. Shutthanandan, D. Gelles, Surf. Coat. Technol. 188–89 (2004) 55–61.
[16] S. Koch, P.V. Hendriksen, T. Jacobsen, L. Bay, Solid State Ionics 176 (2005) 861–869.
[17] S. Koch, P.V. Hendriksen, Solid State Ionics 168 (2004) 1–11.
[18] Y.S. Chou, J.W. Stevenson, R.N. Gow, J. Power Sources 170 (2007) 395–400.
[19] Y.S. Chou, J.W. Stevenson, P. Singh, J. Electrochem. Soc. 154 (2007) B644–B651.
[20] Y.S. Chou, J.W. Stevenson, R.N. Gow, J. Power Sources 168 (2007) 426–433.
[21] K.A. Nielsen, M. Solvang, S.B.L. Nielsen, A.R. Dinesen, D. Beeaff, P.H. Larsen, J. Eur. Ceram. Soc. 27 (2007) 1817–1822.
[22] S.P. Simner, M.D. Anderson, L.R. Pederson, J.W. Stevenson, J. Electrochem. Soc. 152 (2005) A1851–A1859.
[23] S. Megel, K. Eichler, N. Trofimenko, S. Hoehn, Solid State Ionics 177 (2006) 2099–2102.
[24] B.P. McCarthy, L.R. Pederson, H.U. Anderson, X.D. Zhou, P. Singh, G.W. Coffey, E.C. Thomsen, J. Am. Ceram. Soc. (2007).
[25] L.A. Chick, L.R. Pederson, G.D. Maupin, J.L. Bates, L.E. Thomas, G.J. Exarhos, Mater. Lett. 10 (1990) 6–12.
[26] W.J. Quadakkers, V. Shemet, L. Singheiser, USA (2003).
[27] J.W. Stevenson, P.F. Hallman, T.R. Armstrong, L.A. Chick, J Am. Ceram. Soc. 78 (1995) 507–512.
[28] J.A.M. Van Roosmalen, E.H.P. Cordfunke, J.P.P. Huijsmans, Solid State Ionics 66 (1993) 285–293.
[29] J.H. Kuo, H.U. Anderson, D.M. Sparlin, J. Solid State Chem. 83 (1989) 52–60.
[30] J.H. Kuo, H.U. Anderson, D.M. Sparlin, J. Solid State Chem. 87 (1990) 55–63.
[31] M. Mori, Y. Hiei, N.M. Sammes, G.A. Tompsett, J. Electrochem. Soc. 147 (2000) 1295–1302.
[32] E.O. Ahlgren, F.W. Poulsen, Solid State Ionics 86-8 (1996) 1173–1178.
[33] ImageJ for Microscopy, http://rsb.info.nih.gov/ij/.
[34] C.M. D'Souza, N.M. Sammes, J. Am. Ceram. Soc. 83 (2000) 47–52.
[35] A. Atkinson, A. Selcuk, Solid State Ionics 134 (2000) 59–66.
[36] D.L. Meixner, R.A. Cutler, Solid State Ionics 146 (2002) 273–284.
[37] E. Ryshkewitch, J. Am. Ceram. Soc. 36 (1953) 65–68.
[38] D.K. Hale, J. Mater. Sci. 11 (1976) 2105–2141.